Astron. Astrophys. 321, 29–44 (1997)

ASTRONOMY
AND
ASTROPHYSICS

Effects of star cluster evolution on emission line ratios and the application to H II galaxies

Including a calibration of the R_{23} vs. 12+log(O/H) relationship

K. Olofsson

Astronomiska observatoriet, Box 515, S-751 20 Uppsala, Sweden

Received 20 December 1994 / Accepted 22 July 1996

Abstract. A model of spectral evolution of star forming galaxies of various metallicity has been used to study the relation between the optical emission line ratio R_{23}= ([OII]λ3727 +[OIII]$\lambda\lambda$4959,5007)/Hβ and the nebular oxygen abundance. It is shown that the scatter in an empirical comparison sample could be due to various upper stellar mass limits or different slopes of the stellar initial mass function in these objects. However, it is more likely to be an effect of evolution of the underlying stellar population, i.e. the star forming knots observed are of different ages, or equally, the temperature of the ionizing radiation is different. This is particularly evident studying the evolution a few million years after the star formation has ceased. These calculations show that the so called lower branch of the relation is much less sensitive to age than the turn-over region or the upper branch using an instantaneous burst of star formation. This is because massive stars, which dominate the light in a young stellar population, of low metallicity remain at higher effective temperature compared to a star of higher metallicity. In a region of active star formation the R_{23} vs. oxygen abundance relation is even more pronounced since it proves to be very insensitive to age. In the absence of a temperature-sensitive line for the oxygen abundance determination an empirical or semi-empirical approach is normally utilized relying on a calibration of the R_{23} vs. oxygen abundance relation. In this analysis a new calibration of the upper branch, based on a fit of theoretical curves to empirical data of the lower branch, is attempted.

Key words: galaxies: evolution – galaxies: stellar content – galaxies: starburst

1. Introduction

H II region-type objects contain hot unevolved stars and comprise a number of familiar classes. Beside galactic H II regions and extragalactic H II regions in the disk of other spiral galaxies, blue compact and irregular galaxies are also included in this category. The one unifying characteristic of these objects is that their spectra show emission lines with ratios typical of thermal photoionization processes. They evidently contain relatively large amounts of gas. Blue compact and dwarf irregular galaxies are often named starbursts since they form stars recurrently at a prodigious rate over relatively short timescales, i.e. less than a few times 10^7 years. The reason for this bursting nature is probably that they are ionized by a large number of hot OB stars which could have a positive impact on star formation in the vicinity due to self-propagation (Gerola et al., 1980). The energetic output from these stars probably also has a negative feedback on the star formation since ionization fronts (Whitworth, 1979), stellar winds and supernovae explosions (De Young and Gallagher, 1990; De Young and Heckman, 1994) cooperate in order to terminate the episode of star formation. After of the order of a few billion years, depending on their physical sizes (Gerola et al., 1980) and the condition of the intergalactic medium, the gas has reassembled and cooled enough for star formation to recommence triggered by e.g. interaction with neighbouring intergalactic clouds of gas. In the following, extragalactic H II regions, blue compact and irregular galaxies will be referred to as H II galaxies. In the absence of other sources of excitation and ionization such as shock-heating or non-thermal radiation, the physics of these objects is, at least partly, understood in terms of modelling of H II regions (e.g. Stasińska, 1982; Evans and Dopita, 1985; Ferland, 1993). However, due to projection-effects their geometry is often unknown. The content and distribution of internal dust is another problem affecting the interpretation of the observations. Optically, the amount of dust is normally deduced from the Balmer recombination decrement. The chemical abundance of various elements is one of the major properties that can be extracted from spectra of H II galaxies. The abundance determination relies on the possibility to measure the strength of some emission lines in the gas of these galaxies. However, due to the weakness of some crucial lines this often proves to be a difficult task and some other method has to be applied which is one of the scopes of this investigation. The metallicity is one of the most important quantities when

it comes to an understanding of the evolution of objects since it traces the star formation history of the universe. For example, blue compact and irregular galaxies have many properties characteristic of young objects. Deep imaging of a sample of these show no or little signs of the presence of an underlying old stellar population (Kunth et al., 1988). They are gas-rich, have blue colours and, in particular, low metal abundances indicative of being formed later than the generally accepted epoch of galaxy formation at a redshifts of $\sim$ 2-3 (Carlberg and Couchman, 1989; White, 1989). The existence of radial metal abundance gradients in disk galaxies is now widely accepted (e.g. Shields and Searle, 1978; Pagel et al., 1979; Kwitter and Aller, 1981; McCall, 1982; Talent, 1983; Stauffer and Bothun, 1984; Evans, 1986; Garnett and Shields, 1987; Vílchez et al., 1988; Walsh and Roy, 1989; Zaritsky et al., 1990; Martin and Roy, 1992). The trend is that the metallicity increases inwards. One possible interpretation of these results is that the inner parts of spiral galaxies formed earlier than the outer parts. An interesting review of the various problems encircling the topic of chemical abundances in galaxies containing H II regions can be found in Dinerstein (1989).

The abundance of oxygen in the interstellar medium of H II galaxies is particularly interesting to study since, in this type of objects, the emission lines used for the measurements appear relatively strong and well defined, i.e. they are not affected by blending or underlying stellar absorption lines. The latter can be a problem e.g. in determining the helium abundance in the gas and also influences the strength of the hydrogen lines in emission which affects the correction for extinction (Díaz, 1988; Olofsson, 1995a). Moreover, the ionization correction factor for neutral oxygen is believed to be negligible since, in a region of active or post-active star formation, most of the oxygen appears in the O^+ and O^{++} states. The origin of oxygen is mainly believed to be type II supernovae in massive stars, i.e. it is produced and expelled by stars in excess of $\sim$ 10 $M_\odot$ (e.g. Maeder, 1991; Thielemann et al., 1993; Woosley and Weaver, 1995). It is the major element ejected into the interstellar medium in a young burst of star formation assuming that stars are formed over a reasonable mass range, i.e. up to $\sim$ 100 $M_\odot$ (e.g. Pilyugin, 1992; Olofsson, 1995b). Oxygen is also an important coolant of the nebular gas and the lines responsible for the cooling are strongly dependent on the metallicity due to its anticorrelation with the electron temperature (e.g. Masegosa et al., 1994). In the metallicity range of $\sim$ 1/50 to 1/2 $Z_\odot$ the cooling is dominated by the forbidden optical lines [OIII]$\lambda\lambda$4959,5007Å, which peak in strength at $\sim$ 1/5 $Z_\odot$. For lower abundances the strength of these lines decreases due to the underabundance of oxygen atoms. At abundances higher than solar the gradual decrease of the electron temperature results in a shift of the cooling to the [OIII] ^{3}P ground term fine-structure lines in the infrared at 52 and 88μ. A determination of the oxygen abundance normally relies on the temperature- sensitive line ratio [OIII]$\lambda\lambda$(4959+5007)/[OIII]λ4363. However, many extragalactic objects are too faint for a reliable measurement of the strength of the [OIII]λ4363Å line. The variation of the strength of the [OIII]$\lambda\lambda$4959,5007Å lines with oxygen abundance suggests that some relation is at hand which could be useful in the absence of the λ4363Å line. This was realized by Alloin et al. (1979) and Pagel et al. (1979) who suggested that the line ratio R_{23}= ([OII]λ3727 +[OIII]$\lambda\lambda$4959,5007) /Hβ could be used. The [OII]λ3727Å line is much weaker than the [OIII]$\lambda\lambda$4959,5007Å lines in a spectrum of an active region of star formation. This so called "bright-line" method has been used by many investigators (e.g. Pagel et al., 1979; Pagel et al., 1980; Edmunds and Pagel, 1984; McCall et al., 1985; Dopita and Evans, 1986; Torres-Peimbert et al., 1989; Skillman, 1989; McGaugh, 1991) although the empirical calibration in the R_{23} vs. (O/H)-plane has lead to different results, mainly an effect of use of data of various quality and of the method applied. As mentioned, a reliable calibration rests on observations where the λ4363 line is measurable with some confidence. This has in particular been possible for some objects with a 12+log(O/H) (the expression used hereinafter, the solar value has been taken as 8.93 using this notation) of about 7.2-7.9 (Skillman, 1989), mainly because the optical oxygen lines appear strong in this region. This part of the relation is often referred to as the "lower branch" of the R_{23} vs. oxygen abundance relation. For higher abundances the scatter in the empirical sample is much larger resulting in equally large uncertainties in the calibration. An interesting theoretical approach towards an understanding of this problem was taken by McGaugh (1991). He studied how the importance of varying the upper stellar mass limit affected the R_{23} vs. oxygen abundance relation as well as the effect of using a reasonable, with respect to empirical results, range in the ionization parameter. Cerviño and Mas-Hesse (1994) performed an extensive study of the importance of metallicity effects in star forming regions using a model of population synthesis. In particular the effects on the nebular emission line spectrum, Wolf-Rayet and red supergiant stars, the equivalent width of Hβ in emission, the ratio of the strengths of the stellar Si IV and C IV lines in the ultraviolet and the V-K broad-band line indices were investigated. Finally, from their model they estimated the effective temperature of the star clusters in a sample of emission line galaxies. Also, García-Vargas et al. (1995) presented interesting emission line strengths in the optical and infrared using a model of evolutionary synthesis under different assumptions about the metallicity, total mass, hydrogen densities and distance from the ionizing stars.

In this analysis the effects of evolution of single burst stellar populations of various metallicity are investigated. The effects of various slopes of the stellar initial mass function (IMF) and upper stellar mass limits on the R_{23} vs. oxygen abundance relation are tested. Different assumptions on the length of star formation, instantaneous and continuous are studied. Finally, a method of calibration of the upper branch, based on a fit of model data to empirical ones of the lower branch, is performed. Sect. 2 presents the theoretical platform while Sect. 3 is devoted to results and discussion. Conclusions are found in Sect. 4.

2. The theoretical basis

2.1. The model of spectral evolution

A numerical model of spectral evolution has been employed. It is based on model stellar atmosphere spectra and stellar evolutionary tracks. The technique used is the same as the one described in Olofsson (1989) which can be consulted for details. The star formation rate can be assumed to be instantaneous, continuous, constant or exponentially decreasing. The lower and upper stellar mass limits can take any values between 0.1-120 $M_{\odot}$ and any value of the slope of the IMF can be chosen. Any reasonable shape of the IMF can be assumed. The total mass of gas to be transformed into stars and the efficiency of star formation can also be chosen. The output presents fluxes of the calculated stellar population at 1221 wavelength points at various timesteps from 1 Myr up to 20 Gyr. The total number of Lyman continuum photons ejected from the stellar population per unit time is also presented at each timestep. Finally, the resulting spectral energy distribution and the total number of Lyman continuum photons at a given time is used in combination with a model of photoionization in order to calculate the emergent nebular spectrum and in particular relevant emission line ratios. The most important ingredients in spectral evolutionary synthesis are the choice of stellar evolutionary tracks, library of stellar spectra and the photoionization model used.

2.2. Stellar evolutionary tracks

The evolutionary tracks have been taken from calculations by the Geneva-group (Schaller et al., 1992; Schaerer et al., 1993a; Charbonnel et al., 1993). They follow the evolution of massive stars ($M > 7M_{\odot}$) to the end of C-burning. For intermediate mass stars the evolution is traced to the end of the early asymptotic giant branch and for low mass stars ($M < 1.7M_{\odot}$) to the point of the He-flash. These models include convective overshooting and different amounts of mass loss, they also include the Wolf-Rayet phase which is important for stars with relatively high metallicities i.e. higher than $\sim$ 1/3 of the solar value. The models cover the mass range from 0.8 to 120 $M_{\odot}$ and they form therefore a homogeneous grid. This is of great advantage in this kind of work since using data from different sources often introduce uncertainties due to the various assumptions and techniques applied. The metallicities used in this analysis are the following; Z=0.001, 0.004, 0.008, 0.020, the latter represents the solar value. It was necessary to interpolate linearly between these metallicities in order to obtain a closer grid. Due to the lack of reliable stellar evolutionary tracks below Z=0.001 (corresponding to 12+log(O/H)= 7.63) the evolutionary tracks of the Geneva-group were extrapolated down to 7.0, i.e. to Z$\sim$ 0.00023. This was motivated by the existency of rather metal-poor H II galaxies, i.e. down to 12+log(O/H)= 7.24. It could perhaps be regarded as a quite hazardous exercise and is certainly a source of uncertainty even though the evolution especially at high stellar masses, since these are the ones affecting the nebular component the most, is rather smooth comparing tracks of different metallicities. This is especially true using evolutionary tracks of low metallicity since they do not experience the, often complicated, Wolf-Rayet phase which involves strong stellar winds. It is essentially the change in metallicity that modifies the mass loss rate of a high mass star which in turn governs its evolution. Since the mass loss rate decreases with decreasing metallicity it is expected that evolutionary tracks of lower metallicity than Z= 0.001 are rather similar when it comes to effective temperature and luminosity (Maeder, 1995). In support of this it was found that using stellar populations of Z= 0.00023 and 0.001 in order to calculate the emergent nebular emission line ratios (see Sect. 2.4) resulted in a difference in log R_{23} of no more than 3%. The abundance-ratios were assumed to be solar. For masses lower than 0.8 $M_{\odot}$ evolutionary tracks from VandenBerg (1985a, 1985b, and 1986) were used. For tracks of 0.1 and 0.2 $M_{\odot}$ data of pre-main sequence stars were used (Grossman and Graboske, 1971), the pre-main sequence phase was also implemented for stellar models up to 3 $M_{\odot}$ using the calculations of VandenBerg (1985a). It should be clear that stars of low mass have no influence on this kind of work since they are too cool to contribute to the ionizing flux. With this grid at hand models for intermediate stellar masses were lineally interpolated in the log M-t plane following the equivalent evolutionary points technique suggested by Ciardullo and Demarque (1977). The final grid includes a total of 52 evolutionary tracks for each metallicity.

2.3. The library of model stellar spectra

There are many sources of model stellar atmosphere spectra available for spectral synthesis. A perfectly realistic model should allow for a spherical geometry of the star, effects of line blanketing, bound-free transitions of hydrogen and helium as well as heavy elements, effects of stellar winds whenever they are expected to occur and a treatment of convective overshooting and microturbulence. The model atmosphere calculations should be performed under the assumption of non-LTE especially at high effective temperature, they should cover a wide range in effective temperature and effective surface gravity, as well as in metallicity. In order to be useful in spectral synthesis the stellar atmosphere models should also be available over a large enough range in wavelength. Unfortunately, the existing stellar libraries only include some of the desired properties. Hummer and Mihalas (1970) developed model atmospheres under LTE conditions where they also studied the effects of various stellar surface gravities and chemical compositions. Mihalas (1972) presented non-LTE models. One shortcoming with these models is the quasi-treatment of the inclusion of heavy elements. Clegg and Middlemass (1987) presented non-LTE model atmosphere calculations for $T_{eff} \geq 40000$K and some relevant stellar surface gravities. However, only hydrogen and helium opacity sources were included which therefore hampers the use of these models in the study of populations of various metallicity. Kurucz (1992) presented new LTE model atmospheres based on his old set Kurucz (1979). The advantage of using this set of models is the wide range in effective temperature, surface gravity and, in particular, chemical composition. Howarth and

Lynas-Gray (1989) calculated a grid of LTE model atmosphere spectra based on the code of Kurucz. These models provide a wider range in stellar surface gravity at high effective temperatures compared to the grid of Kurucz. The effect of using ionizing sources of different chemical abundance on the emergent spectral energy distribution has been discussed by e.g. Hummer and Mihalas (1970), Skillman (1989) and Evans (1991). A decrease of the metallicity in the atmosphere of a star results in a decrease of the ionization edges which in turn results in a hardening of the radiation field since the discrepancies in the emergent fluxes are more pronounced in the far-ultraviolet They are also more important for smaller values of the surface gravity. Although the luminosity of the stars producing the ionizing photons (stars hotter than $T_{eff} \sim$ 30000K) are all mostly on the main sequence, large variations in luminosity are expected studying e.g. the most recent evolutionary tracks developed by the Geneva-group (Schaller et al., 1992; Schaerer et al., 1993a; Schaerer et al., 1993b; Charbonnel et al., 1993). The stellar surface gravity has great influence on the emergent spectral energy distribution, especially in the far-ultraviolet and for temperatures in excess of $\sim$ 40000K (Hummer and Mihalas, 1970). A decrease of the surface gravity resembles that of an increase in effective temperature of the radiation field. It is clear that the use of any of these sources of model atmosphere spectra will result in some uncertainties. It is felt that the use of the Kurucz (1992) models, even though they apply only under LTE conditions, offer the best choice in modelling H II regions. This is in line with the conclusion reached by Skillman (1989) and Evans (1991). The obvious advantage is the wide range in basic stellar parameters. They form therefore a unique homogeneous set of models, while the others mentioned above, are somewhat limited especially when it comes to their range in effective temperature. The disadvantage of using Kurucz' models is the assumption about LTE. However, studying derived mean effective temperatures of star clusters, hereafter labelled the temperature of the ionizing radiation, T_{ion}, of the ionizing source in H II galaxies, one find that a majority of the objects presented are in the range of 35000-45000K (Cerviño and Mas-Hesse, 1994). Although non-LTE effects are important at these temperatures they become severe only at higher effective temperatures. This is especially true using models with subsolar chemical abundances (Skillman, 1989) which is the case in this analysis. An elaborate discussion on the importance of the effects of non-LTE can be found in Kudritzki et al. (1991). The most crucial point for this kind of analysis is how the choice of model stellar atmosphere affects the strength of the emission lines appearing in the expression for R_{23}. This was visualized by Skillman (1989) who studied the ratio [OII]/[OIII] (his Fig. 12). One sees that the choice of stellar atmosphere is of less importance in determining the ratio of these lines if the temperature of the ionizing source is in excess of $\sim$ 40000K. The comparison was made using the models of Hummer and Mihalas (1970) and Kurucz (1979) at the same effective temperature, surface gravity and chemical abundance. A recent review of existing stellar libraries, theoretical as well as empirical, can be found in Olofsson (1996).

In this investigation model stellar atmosphere spectra for use in evolutionary synthesis of galaxies have been taken from the updated grid of Kurucz (1992). These improved models include new line and continuous opacities as well as some treatment of convective overshooting. The grid covers a wide range in metallicity (six orders of magnitude) well within the one occupied by H II galaxies. Needless to say, the metallicities used for the spectra were the same as the ones chosen for the evolutionary tracks. Additional spectra at intermediate metallicities were extracted by linear interpolation. The range in effective temperature is 3500-50000K. At temperatures above $\sim$ 40000K model stellar atmospheres from Howarth and Lynas-Gray (1989) were also used due to the restricted range in stellar surface gravity in the grid of Kurucz. From a comparison with the temperatures derived from the evolutionary tracks (Sect. 2.2) it is obvious that an extrapolation to higher effective temperatures is necessary. This will introduce some uncertainties but a solace is that spectra at these high temperatures are rather featureless and nothing drastically occurs in the atmosphere of stars between, say, 50000 and 60000K. A comparison was made on how the use of a model derived by Clegg and Middlemass (1987) at T_{eff}= 60000K and log g= 4.5 and one extrapolated to the same effective temperature and stellar surface gravity of Howarth and Lynas-Gray (1989) affected the value of R_{23}. It was found that the difference in R_{23} was about 7%. The range in the logarithm of the surface gravity is 0.0-5.0, mostly within the range occupied by the evolutionary tracks used. The wavelength coverage is 90.9Å to 0.16mm, which is the range used in this investigation. The spectral resolution varies depending on the wavelength. In the far-UV the resolution is typically a couple of Å, in the optical it is 20Å while in the far-IR it is much worse but still acceptable for determining the spectral energy distribution. In order to account for changes along a given evolutionary track a method of linear interpolation was applied. This concerns the surface gravities as well as the effective temperatures.

2.4. The nebular component

The nebular emission line ratios were calculated with the use of the code CLOUDY (Ferland and Truran, 1981; Ferland, 1993). Generally, the spectrum of an H II region is determined by the chemical abundance of the nebular gas, the spectral energy distribution of the ionizing source(s) or equally,the T_{ion}, and the geometry of the gaseous cloud normally expressed using the ionization parameter U. In this analysis the spectral energy distribution of the emergent model stellar population was used as input. For each timestep the number of Lyman continuum photons per unit time, $Q(H)$, was calculated by integrating shortwards of the Lyman limit at 912Å. This number is directly proportional to the ionization parameter through the relation

$$U = \frac{Q(H)}{4\pi r^2 N c}$$

N is the number density of the gas, a typical value for H II galaxies is 100 cm^{-3} which is the number used here. r is some inner radius, in this case it is the distance between the ioniz-

ing source and, the assumed, spherical cloud. c is the speed of light. Since the number of Lyman continuum photons is used as an input parameter the ionization parameter is calculated at each time-step. It is also assumed that the filling factor of the nebular gas is unity. This quantity affects the emissivity of the cloud since e.g. a low filling factor means that fewer atoms are available for absorption of the emergent radiation. This approach is acceptable for this kind of work but it is clear that a study of individual objects requires a specific assumption about the geometry, a property which is measurable at least to a first approximation. However, the distribution of gas is difficult to determine in extragalactic objects but it is known from studies of galactic H II regions, which provide high spatial resolution, to be filamentary and clumpy.

2.5. Miscellaneous

The final grid in metallicity of the stellar as well as nebular components is contained in the interval $7.0 \leq$ 12+log(O/H) $\leq$ 9.0 and presented in steps of 0.2. It is assumed that each stellar population and its nebular component have the same metallicity which is a fair assumption when the star forming region is young. The resolution in time is 1 Myr and the evolution between 1 and 15 Myr is studied assuming a single burst of star formation. Finally, it should be noted that no method of smoothing or curve fitting has been applied to any of the results presented. It is clear that an insufficient number of evolutionary tracks (masses) results in non-physical "jumps" in e.g. colours and magnitudes as stars move into different evolutionary stages (e.g. Charlot and Bruzual, 1991). The use of 52 tracks in this investigation ensure a rather smooth behaviour of the flux distribution as a function of time.

3. Results and discussion

3.1. The empirical comparison sample

The comparison sample consists of data of H II regions in nearby disk galaxies, blue compact and irregular galaxies. Two sets of data have been used and it is important to realize that the oxygen abundance has been determined with the use of the [OIII]λ4363Å line in all these objects. The first set is taken from the compilation of McGaugh (1991) where the various sources are presented. For the sake of convenience the authors are listed here as well (Pagel et al., 1979; Pagel et al., 1980, Kinman and Davidson, 1981; Kunth and Sargent, 1983; Webster and Smith, 1983; Edmunds and Pagel, 1984; Davidson and Kinman, 1985; Peimbert et al., 1986; Campbell, 1988; Skillman et al., 1988; Skillman et al., 1989a; Skillman et al., 1989b; Torres-Peimbert et al., 1989; Salzer et al., 1991). The objects belong to all three classes given above. It should be clear that this set of data is rather heterogeneous since the authors have used different methods of reduction and analysis. Typical errors reported in the log(O/H) are at the most 0.1-0.2 dex. The second set is more homogeneous and is derived from Masegosa et al. (1994) which in turn is based on the spectrophotometric catalogue of Terlevich et al. (1991). All of these objects are in the category of blue compact and irregular galaxies. Errors in the measurement of oxygen abundances are not given but median error estimates of the [OIII]$\lambda\lambda$4959,5007Å lines are about 5%. 15% is reported for the [OIII]λ4363Å line. This gives somewhat smaller errors in the log(O/H) compared to the former sample. It should be emphasized that Masegosa et al. rejected objects with emission lines affected by Wolf-Rayet stars and shock excitation. Moreover, there are no indications that non-thermal sources contribute to the radiation in any of the objects in the two samples. The total sample is visualized in Fig. 1 and it is obvious that most objects are situated such that $\log R_{23} \geq 0.8$ and $7.9 \leq$ 12+log(O/H) ≤ 8.3, roughly. This is most certainly a selection effect since the optical [OIII] lines are the strongest in this area (see the Introduction), often referred to as the "turn-over region". The scatter in R_{23} for a given oxygen abundance in this region is also large. The region above 12+log(O/H)$>$ 8.3, the so called "upper branch", is quite sparsely populated because, for reasons already stated, the [OIII]λ4363Å line is very weak or absent and whenever measurable the uncertainties are often large. As evident from the figure, this relation is double-valued and results in ambiguities in the determination of the oxygen abundances. However, Alloin et al. (1979) suggested that the optical oxygen-over-nitrogen emission line ratio [OIII]/[NII] could be used in separating the two branches.

The value of R_{23} can be seriously affected by the correction for internal dust using the Balmer decrement. Masegosa et al. (1994) used the Hγ/Hβ emission line ratio for determining, and correcting for, internal extinction, since the normally used Hα/Hβ-ratio was affected by second-order contamination in the red.

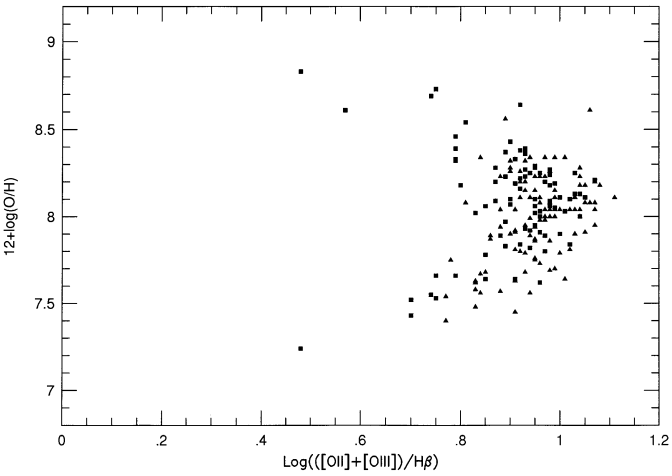

Fig. 1. The empirical $\log R_{23}$= log(([OII]λ3727 +[OIII]$\lambda\lambda$4959, 5007)/ Hβ) versus oxygen abundance relation. The comparison sample consists of two sources of data. The first is derived from the compilation of McGaugh (1991) and is presented with filled squares (the individual authors are given in the text) Typical error in the oxygen abundance determination is 0.1-0.2 dex. The second set, presented with filled triangles, is taken from Masegosa et al. (1994) which in turn is based on the spectrophotometric catalogue of Terlevich et al. (1991). Here the errors are somewhat smaller than in the former sample. It should be noted that the oxygen abundance has been determined with the use of the [OII]λ4363Å line in all these objects.

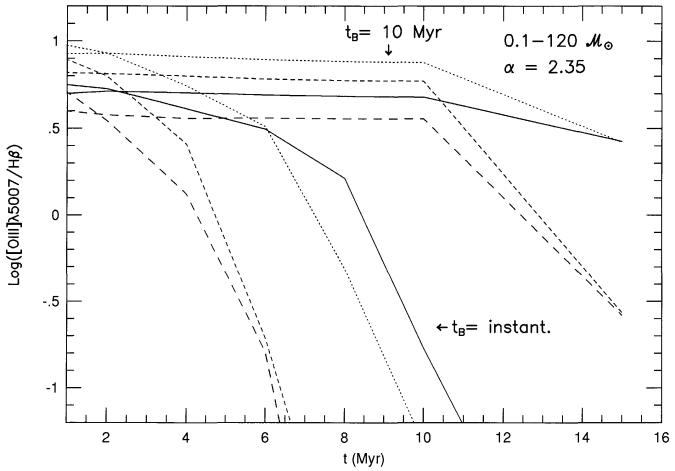

Fig. 2. The figure shows the evolutionary effects on the [OIII]λ5007/Hβ emission line ratio. A Salpeter (1955) slope of the IMF (α= 2.35) and the whole available stellar mass range has been used. Two different lengths of the star formation have been assumed; one instantaneous and one lasting 10 million years. The figure shows the evolution using stellar populations of four different metallicities; Z=0.001 (——), =0.004 (···), =0.008 (– –), =0.020 (— —). These numbers correspond to oxygen abundances of 12+log(O/H)= 7.63, 8.23, 8.53, 8.93. The latter value corresponds to the solar oxygen abundance.

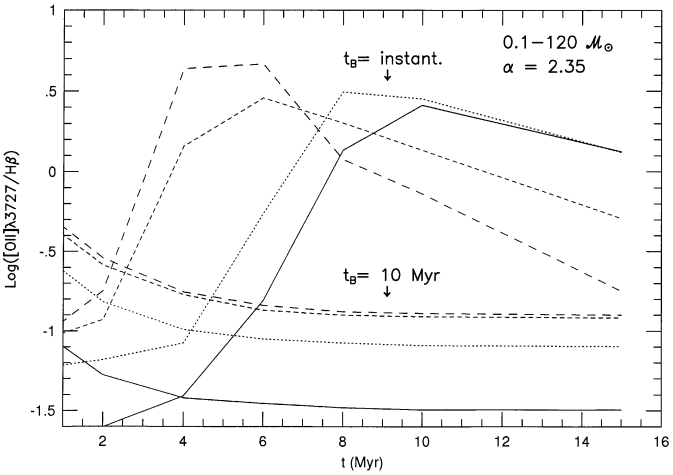

Fig. 3. The evolution of the emission line ratio [OII]λ3727/Hβ. The IMF and assumptions on the length of star formation are as in Fig. 2. The curves represent different metallicities and have the same meaning as in Fig. 2.

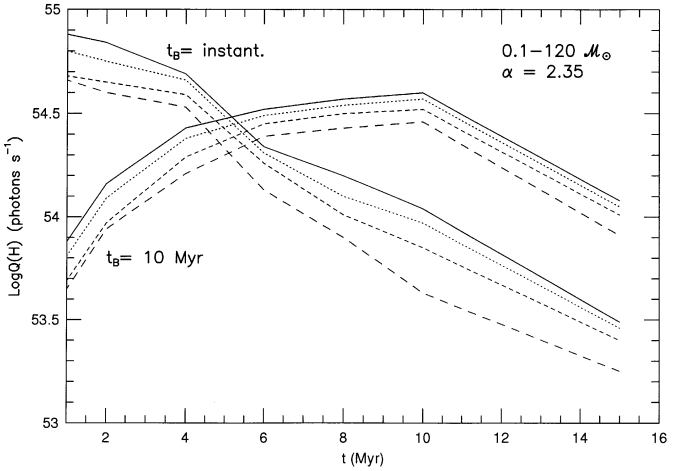

Fig. 4. Effects of temporal evolution on the total number of Lyman continuum photons, $Q(H)$, emitted from stellar populations of various metallicities. The total mass of gas transformed into stars is 10^{10} $M_{\odot}$. The IMF and assumptions on the length of star formation are as in Fig. 2. The curves represent different metallicities and have the same meaning as in Fig. 2.

It is well known that using the Hγ/Hβ lines often results in larger extinctions than if the Hα/Hβ-ratio is used. This is probably due to a larger amount of stellar absorption underlying the Hγ line (Díaz, 1988; Olofsson, 1995a). However, using the former ratio results in a larger correction which consequently somewhat decreases the strength of the [OIII]$\lambda\lambda$4959,5007Å lines with respect to Hβ and increases the strength of the [OII]λ3727Å line. The effect on the latter can be important due to the difference in wavelength between this line and Hβ. It is clear that the value of R_{23} can be affected by various amounts since it is composed of the strength of these separate lines. The problem of a possible overestimation of the interstellar reddening in the sample of Masegosa et al. was also discussed by Cerviño and Mas-Hesse (1994). Other possible sources of error involve non-linearities in the detectors used or some contribution from non-thermal radiation or shock excitation. For example, Seyfert 2 galaxies are known to have [OIII]λ5007/Hβ ratios in excess of 10.

3.2. The length of the burst of star formation

This analysis focuses only on the active and post-active phases of a single burst of star formation of various metallicity since at later ages the residing stellar population is too cool to excite and ionize the interstellar medium. An active region of star formation is revealed through the appearance of a nebular emission spectrum if the stellar mass spectrum involves stars hotter than $\sim$ 30000K, or equally, stars of high enough mass. It is important to realize that star formation can be active without showing emission lines if the stellar mass spectrum is truncated at the high mass end. This is the case in e.g. T Tauri associations. Since this investigation is based on a study of the temporal evolution of emission lines, the presence of these will be used as a tracer of active star formation. Studying the spectral evolution as a function of age (Olofsson 1989, his Fig. 6) it is noticeable that ongoing star formation is characterized by the strong optical [OIII] lines compared to e.g. the Hβ line. Once the star formation is halted the line ratio [OIII]λ5007/Hβ decreases drastically due to the rapid evolution of the most massive stars. The subsequent post-active phase is characterized by the relatively strong [OII]λ3727Å and Hα lines. At later ages, and lasting some 10^8 years or so, the stellar population resembles that of A-stars without a nebular component. This situation prevails even if the starburst is superimposed on an older stellar population provided the strength of the burst is high enough (Bica et al., 1990). An arbitrary definition of the end of the post-active phase could be

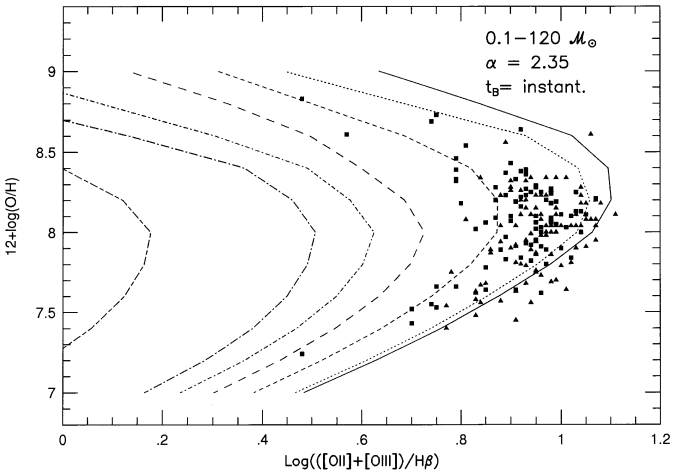

Fig. 5. The R_{23} versus oxygen abundance relation. The curves represent the theoretical temporal evolution of R_{23} using an instantaneous burst of star formation. The curves have the following meaning; 1 10^6 yr (——), 2 10^6 yr (· · ·), 4 10^6 yr (– –), 6 10^6 yr (— —), 8 10^6 yr (– · –), 10 10^6 yr (— · —) and 15 10^6 yr (— – —). The IMF parameters are as stated. The comparison sample is described in the text as well as in Fig. 1.

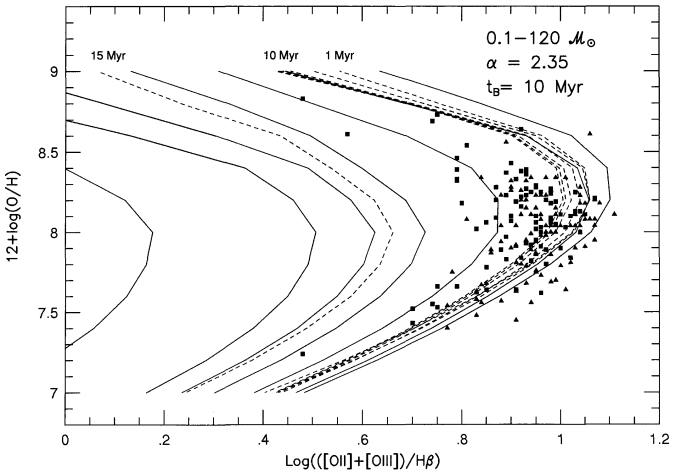

Fig. 6. The effect of a non-instantaneous burst of star formation on the R_{23} versus oxygen abundance relation. The length of star formation is taken as 10 Myr and the evolution between 1 and 15 Myr is presented with dashed curves. The temporal evolution of R_{23} is from the right to the left in the figure. The particular ages are the same as in Fig. 5 and some are marked out for reason of clarity. For the sake of comparison the instantaneous burst case is also given and is represented by the solid curves. The empirical comparison sample and the IMF parameters are the same as in Figs. 1 and 5, respectively.

such that the excitation parameter, i.e. the emission line ratio [OIII]λ5007/Hβ, is less than one.

Studying Fig. 2 one then sees that the post-active phase is terminated some $\sim$ 2-10 Myr after the active star formation itself is halted. This is dependent on the metallicity and the IMF used. Fig. 2 also shows that in a region of active star formation the [OIII]λ5007/Hβ-ratio is kept rather constant and decreases only slightly as a function of time. It is clear that this line ratio is the highest at the intermediate abundance 12+log(O/H)$\sim$ 8.2 while using the solar abundance results in the lowest [OIII]λ5007/Hβ-ratio. As a consequence of the difference in their atomic transition probabilities the [OIII]λ4959Å line is about a factor of three weaker than the λ5007Å line (e.g. Osterbrock, 1989). The line ratio [OII]λ3727/Hβ shows a different behaviour. Fig. 3 indicates that it is rather constant in an active region of star formation, although weak in comparison to the [OIII] lines. In the instantaneous burst case it peaks some 4-10 Myr after the cessation of star formation and is a consequence of its lower state of ionization compared to [OIII]. Comparing calculations at different metallicities one sees that this line ratio is the weakest when the abundance of oxygen is low while in a region of roughly solar abundance it becomes stronger. It is also clear from the calculations that the [OII]λ3727Å line diminishes after some 20-30 Myr after the star formation has ceased which could also mark the termination of nebular emission. The Lyman continuum flux, which is proportional to the number of Lyman continuum photons emitted from an ionization source, is responsible for the excitation and ionization of the interstellar medium. This quantity becomes important for stars with effective temperatures in excess of $\sim$ 30000K. From the extensive discussion in Sect. 2.3 it is clear that the number of ionizing photons derived from a particular model stellar atmosphere is much dependent on the treatment of ionization edges shortward of the Lyman limit which in turn is dependent on the inclusion of bound-free transitions of hydrogen, helium as well as heavy elements. The dependence of the ionizing flux on luminosity, or equally, effective surface gravity was checked. A difference of about 7% was found assuming an effective temperature of 45000K and using the range of effective surface gravities given by the evolutionary tracks. This is valid for stars of solar chemical abundance. At higher effective temperature the difference is smaller. The number of ionizing photons is also dependent on the rate of mass loss for high mass stars. This number drops rapidly for stellar masses larger than $\sim 80\ M_\odot$ in case of no mass loss (Melnick et al., 1985). It is evident that once the star formation is halted the Lyman continuum flux decreases rapidly due to the relatively short lifetimes of the hot OB-stars. It is shown in Fig. 4 that the number of Lyman continuum photons has decreased a factor of $\sim$ 2-4, depending on the metallicity, only 6 Myr after the episode of star formation has ceased. This is valid assuming a Salpeter (1955) slope of the IMF and an upper mass limit of 120 $M_\odot$. It is assumed that the total mass of gas transformed into stars is $10^{10}\ M_\odot$ and it should be clear that this number is directly proportional to the total number of Lyman continuum photons emitted. Once the star formation is halted the decrease in this number is practically monotonous. Some irregularities are seen in the figure and is a consequence of the use of discrete masses in the calculations. One can also note that model stellar populations of low metallicities emit the most Lyman continuum photons. This is because the atmosphere of stars of low metallicity are less opaque and therefore run at higher temperatures. They also have slightly smaller radii.

It should be obvious from this discussion that the length of star formation has bearing on the emergent emission line spectrum and for this reason two different choices were made. One instantaneous and one lasting 10 Myr. The result of using an instantaneous starburst model can be viewed in Fig. 5. The IMF parameters are those given in the figure. The curves represent various ages, from 1 to 15 Myr, and the temporal evolution is from right to left. The distance between the ionization source and the gaseous cloud is adjusted to fit, roughly, the outer envelope of the empirical data. Some interesting details can be noted. The evolution of R_{23} along the lower branch, at a given oxygen abundance, is slower compared to the turn-over or upper branch. For example, studying the ages at 2 and 4 Myr at 12+log(O/H)=7.4, 8.2 and 8.8 reveal that the differences in the logR_{23} are 0.099, 0.184 and 0.185, respectively. The physical reason behind this behaviour can be found in the theory of stellar evolution. Studying the evolutionary tracks of the Geneva-group (see Sect. 2.2) for high stellar masses, since these are the ones contributing the most to the Lyman continuum flux in a young burst of star formation, at different metallicities one sees that a star of lower metallicity remains at a higher effective temperature during the first few million of years of evolution compared to a star of high metallicity. This is also visible studying Fig. 2 in the case of an instantaneous burst of star formation and is in line with the conclusion reached by Cerviño and Mas-Hesse (1994). It is evident that the decline in the high temperature-sensitive line ratio [OIII]λ5007/Hβ is much more rapid for a metallicity close to the solar compared to a low metallicity population. The opposite is true looking at the [OII]λ3727/Hβ line ratio in Fig. 3 where the solar metallicity case peaks earlier than stellar populations and nebular components of lower metallicity. This can in fact explain the scatter in the turn-over region as being an effect of evolution i.e. the star forming knots are of slightly different ages i.e. the T_{ion}'s are different. It should be pointed out that part of the scatter could be an effect of various filling factors in these objects. Using a Salpeter slope of the IMF and an upper mass limit of 120 $M_{\odot}$ but reducing the filling factor 20 times results in a decrease of R_{23} by $\sim 10\%$ at the age of 1 Myr. Fig. 6 shows the R_{23} vs. oxygen abundance relation in the case of continuous star formation. The dashed curves show the evolution using a model with a burst of star formation lasting 10 Myr. The IMF parameters are the same as in the instantaneous burst case. As indicated by the previous results on the separate line ratios, the evolution is rather slow in this case. When the star formation is halted, at the age of 10 Myr, R_{23} declines significantly over a period of 5 Myr. Finally, it can be noted that, comparing the instantaneous burst case with the one lasting 10 Myr, results in about 4% higher value for logR_{23} in the former case. This is because the efficiency of the star formation was taken to be the same in both cases resulting in a higher star formation rate using an instantaneous burst of star formation.

3.3. Variations in the IMF

The IMF is normally expressed as a simple power-law $\Phi(m) \propto m^{-(1+x)}$ where Φ is the fraction of the total number of stars of mass m formed per unit mass interval. In the following the exponent is expressed as α=1 + x where α= 2.35 is the value derived by Salpeter (1955). Whether the stellar IMF is universal or not has been dwelled upon during the last decade or so (e.g. Scalo, 1986; 1987). Particularly important for this kind of exercise is the question of whether some star forming regions are "top-heavy", i.e. have stellar masses much in excess of 100 $M_{\odot}$ (Scalo, 1990). If this is the case these stars would certainly have an influence on the temperature-sensitive lines [OIII]$\lambda\lambda$4959,5007Å in the sense that they would increase in strength. A slope of the IMF more flat than the Salpeter one has the same effect. As mentioned earlier, the value of R_{23} derived from the spectrum of an H II galaxy is, in particular, determined by the T_{ion} of the stars in the cluster. It should be clear that lowering the upper mass limit or flattening the slope of the IMF mimics a decrease of the ionization temperature. This is because the most massive stars are also the ones with the highest effective temperature. It would therefore be difficult to disentangle an evolved star forming region from a genuinely young one formed with a suppressed upper mass limit from an optical spectrum alone. In this analysis two different slopes of the IMF have been used; α= 1.35 (flat case) and α= 2.35 (Salpeter case). Four different upper mass limits have been accounted for; 30, 60, 100 and 120 $M_{\odot}$. The lower mass limit has been taken as 0.1 $M_{\odot}$ in all calculations, it was found that an increase of this number to 3 or 10 $M_{\odot}$ has only minor effects on the R_{23} emission line ratio since, in an active burst of star formation, mostly massive stars are contributing to R_{23}. The evolution using a slope of the IMF of α= 1.35 is shown in Fig. 7a with dashed curves. The results using a Salpeter slope is given for comparison with solid curves. The main effect of using a more flat slope of the IMF is that the relative amount of massive stars becomes higher which increases the value of R_{23}. Indeed all curves representing the ages are shifted to the right in the figure without affecting their shape. Fig. 7b shows the result of lowering the upper mass limit from 120 to 100 $M_{\odot}$. The latter choice is shown with dashed curves. The effect on R_{23} is only minor and one can note that from the age of 4 Myr and later the curves coincide. This is because a lowering of the upper mass limit has the same effect as that of evolution. Temporal evolution, using an instantaneous burst of star formation, is simply a depopulation of the mass function starting with the most massive stars and shortest lifetimes. Fig. 7b reveals that at the age of 4 Myr the mass function is depopulated in such a fashion that only stellar masses of 60 $M_{\odot}$ and less remain (compare the evolutionary tracks used) and the subsequent evolution in both cases will follow the same pattern. In consequence, a model with an upper mass limit of 60 $M_{\odot}$ (Fig. 7c) shows the same behaviour as in the previous case although the curves at the age of 1 and 2 Myr are shifted to the left in the figure. Using an upper mass limit of 30 $M_{\odot}$ (Fig. 7d) indicates that the curves coincide with the 120 $M_{\odot}$ model at the age of 6 Myr for the same reason as given above. In conclusion, these results show that if the upper mass limit, initially, is lower than $\sim$ 40 $M_{\odot}$, no evolution of the cluster is evident during the first 5 Myr. The data also seem to constrain, assuming a Salpeter

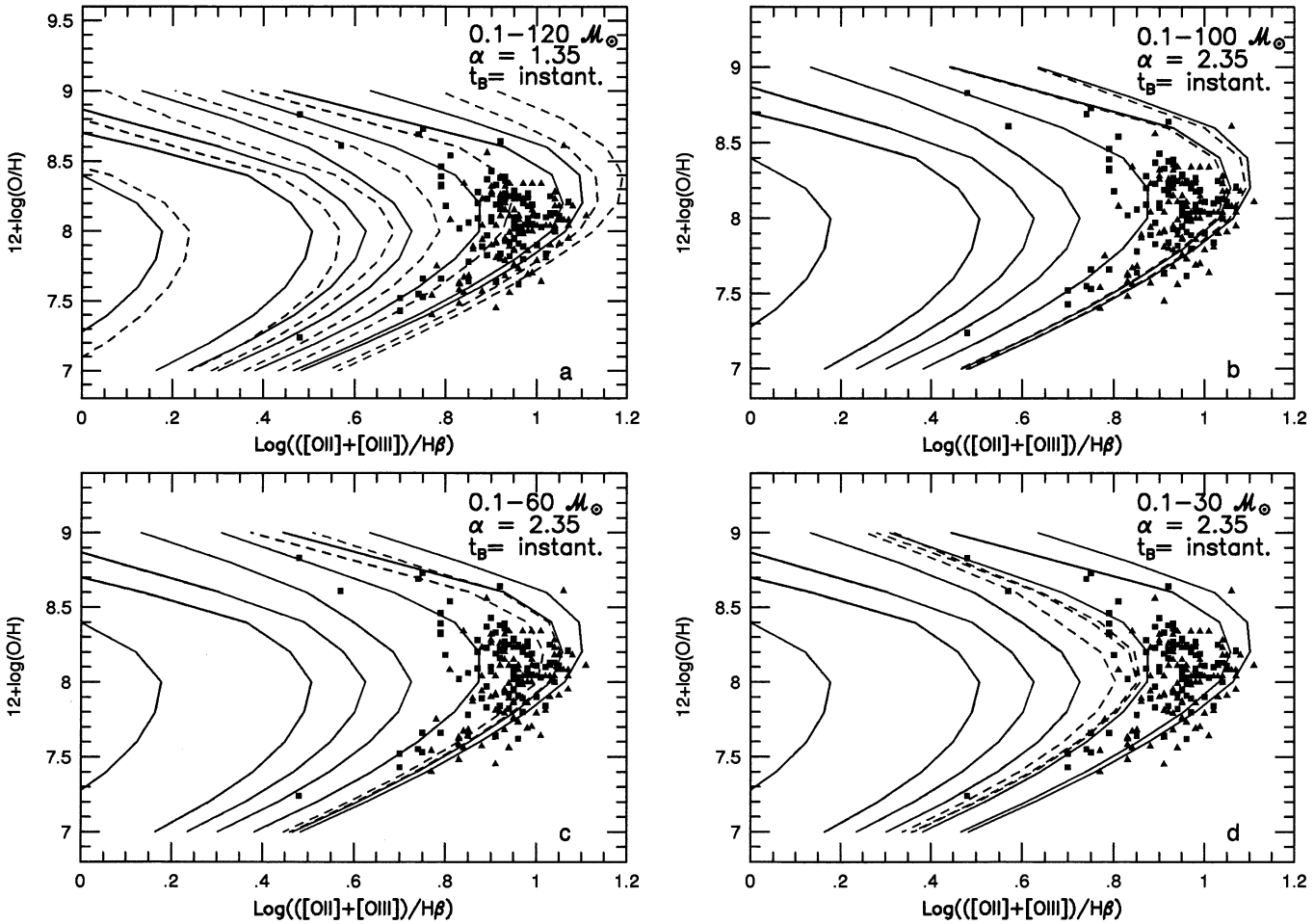

Fig. 7a–d. The R_{23} versus oxygen abundance under different assumptions about the slope of the IMF and the upper mass limit. An instantaneous burst of star formation is used in all cases and the empirical comparison sample is the same as in Fig. 1. Fig. 7a shows the evolution using a relatively flat slope of the IMF, α= 1.35 (dashed curves). The evolution is from right to left in the figure and the age range is between 1 and 15 Myr, the particular ages are the same as in Fig. 5. The Salpeter slope case (α= 2.35) is given for comparison (solid curves). Fig. 7b shows the result of using a Salpeter slope of the IMF and upper mass limit of 100 $M_\odot$ (dashed curves). The model with an upper mass limit of 120 $M_\odot$ is presented for comparison (solid curves). Fig. 7c presents a model with an upper mass limit of 60 $M_\odot$. The model with an upper mass limit of 120 $M_\odot$ is given for comparison (solid curves). Fig. 7d presents a model with an upper mass limit of 30 $M_\odot$. The model with an upper mass limit of 120 $M_\odot$ is shown for comparison (solid curves).

slope of the mass function, the upper mass limits of the objects to 30-60 $M_\odot$.

3.4. Calibration of the R_{23} vs. oxygen abundance relation

As mentioned in the Introduction, the relative abundance of oxygen can be retrieved either by using the temperature-sensitive method, resting on the relatively weak [OIII]λ4363Å line, or by using the "bright-line" method relying on a calibration of the R_{23} vs. oxygen abundance relation. The temperature-sensitive line method is applicable on the lower branch of the R_{23} vs. oxygen abundance relation. As the abundance of oxygen increases, the strength of the optical oxygen lines weakens as the cooling becomes dominated by lines in the infrared. This causes severe problems for the determination of the abundance of oxygen in H II regions in relatively nearby disk galaxies. They are known to have experienced a long history of star formation and have therefore built up a relatively high amount of heavy elements, i.e. they are probably situated on the upper branch of the R_{23} vs. oxygen abundance relation. The problem of weak emission lines for a determination of chemical abundances, whether on the lower or upper branch, applies of course to any star forming galaxy if faint or distant enough. In this section a calibration of the upper branch is attempted based on a fit of theoretical curves to empirical data on the lower branch.

3.4.1. The theoretical age vs. T_{ion} relation

As discussed in Sect. 3.2, the location of the theoretical curves in the R_{23} vs. oxygen abundance diagram (Figs. 5 and 6) is very much dependent on the age of the stellar population, i.e. on the T_{ion} of the star cluster. The age of the stellar popula-

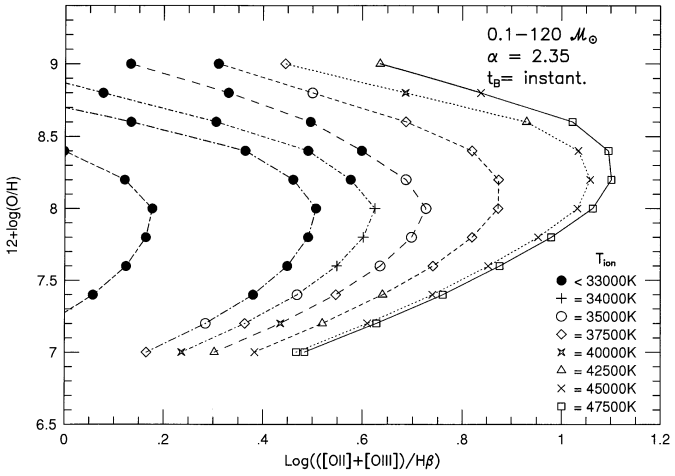

Fig. 8. The curves represent the theoretical temporal evolution of R_{23} using an instantaneous burst of star formation and have the same meaning as in Fig. 5. The IMF parameters are as stated. The corresponding temperature of the ionizing radiation, T_{ion}, of the stellar population is given along each track defined by the symbols given in the legend.

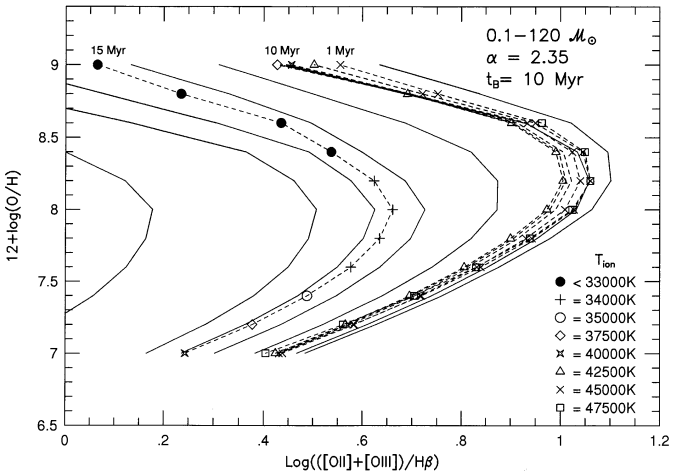

Fig. 9. The effects of a non-instantaneous burst of star formation on the R_{23} versus oxygen abundance relation. The length of star formation is taken as 10 Myr and the curves have the same meaning as in Fig. 6. For the sake of comparison the instantaneous burst case is also given and is represented by the solid curves. The IMF parameters are as stated. The corresponding T_{ion} of the stellar population is given along each track defined by the symbols given in the legend.

tion can not be determined *a priori* but the T_{ion} is possible to extract, at least to a first approximation. It can be determined by fitting observed emission line ratios of a large number of elemental species of different ionization stages to those of photoionization model calculations (e.g. Stasińska, 1982; Evans and Dopita, 1985; Ferland, 1993). Stasińska (1980) suggested that the T_{ion} could be determined in H II regions in which the emission line [OIII]λ4363Å could be measured with some confidence. She studied the theoretical relation between the line ratio [OIII]λ4363/[OIII]$\lambda\lambda$(4959+5007) and the relative oxygen abundance and found a clear distinction between curves of different T_{ion}. The [OIII] line ratio was later named R_{33}. This relation indicated that the value of R_{33} increases as the relative oxygen abundance decreases which was expected from an empirical sample of H II regions. It is also possible to extract the T_{ion} on basis of a measurement of the strength of some oxygen and sulphur emission lines. Vílchez and Pagel (1988) suggested that the radiation softness parameter η= (O^+/O^{++})/(S^+/S^{++}) could be used. The lines involved are the optical [OII]λ3727,3729, [OIII]$\lambda\lambda$4959,5007, [SII]λ6717,6731 and the far-red [SIII]$\lambda\lambda$9069,9532 lines. It is claimed that the η parameter is practically reddening independent as well as density independent if 10^4 cm^{-3} or lower, which is normally the case in H II galaxies. Most important, it is relatively insensitive to the chemical composition which is useful in the calibration of the R_{23} vs. oxgygen abundance relation which is based on the T_{ion} (see Sect. 3.4.3.)

In this analysis the T_{ion} of each model stellar population was determined by comparing the spectral energy distribution shortwards of the Lyman limit at a given age and metallicity with model stellar atmosphere spectra of Kurucz (1992) and Howarth and Lynas-Gray (1989) at the corresponding metallicity in the temperature range 33000-55000K and log g= 4.0-5.0. This was accomplished by using a method of least square summation to the following effective stellar temperatures; 33000, 34000, 35000, 37500, 40000, 42500, 45000, 47500, 50000 and 55000K. These are the temperatures available in the grids of model atmosphere fluxes of Kurucz (1992) and Howarth and Lynas-Gray (1989) except the one at 55000K which was extrapolated (see Sect. 2.3). The result of this exercise is depicted in Fig. 8 for the instantaneous burst model with a Salpeter (1955) slope of the IMF and an upper mass limit of 120 $M_\odot$. The curves correspond to ages 1 to 15 Myr. (cp. Fig. 5). It is clear that a certain age does not correspond to the same T_{ion} over a wide range of oxygen abundance studied. This is especially noticeable at higher oxygen abundances, i.e. at the upper branch, where the temperatures are consistently lower at a given age. The same situation is shown in Fig. 9 for the model with a burst of star formation lasting 10 Myr (cp. Fig. 6). One can note from these two figures that the highest T_{ion}, with the given IMF parameters, is 47500K at the very beginning of the phase of star formation. Some kind of calibration of the R_{23} vs. oxygen abundance relation should therefore rely on the T_{ion} of each object to be studied since, once determined, the value of R_{23} gives, uniquely, the abundance of oxygen.

3.4.2. The T_{ion} of the empirical sample

In order to retrieve the T_{ion} of a star cluster the spectral energy distribution must be normalized since the number of Lyman continuum photons, $Q(H)$, is proportional to the number of ionizing stars. $Q(H)$ can be calculated for each object if the distance and the flux in e.g. the Hβ line are known. This information gives the luminosity in Hβ, L(Hβ), and by applying the expression given by Osterbrock (1989), $Q(H)$= 2.092 10^{12} L(Hβ), the number of Lyman continuum photons can be extracted. The method for determining the T_{ion} of the cluster of stars used in

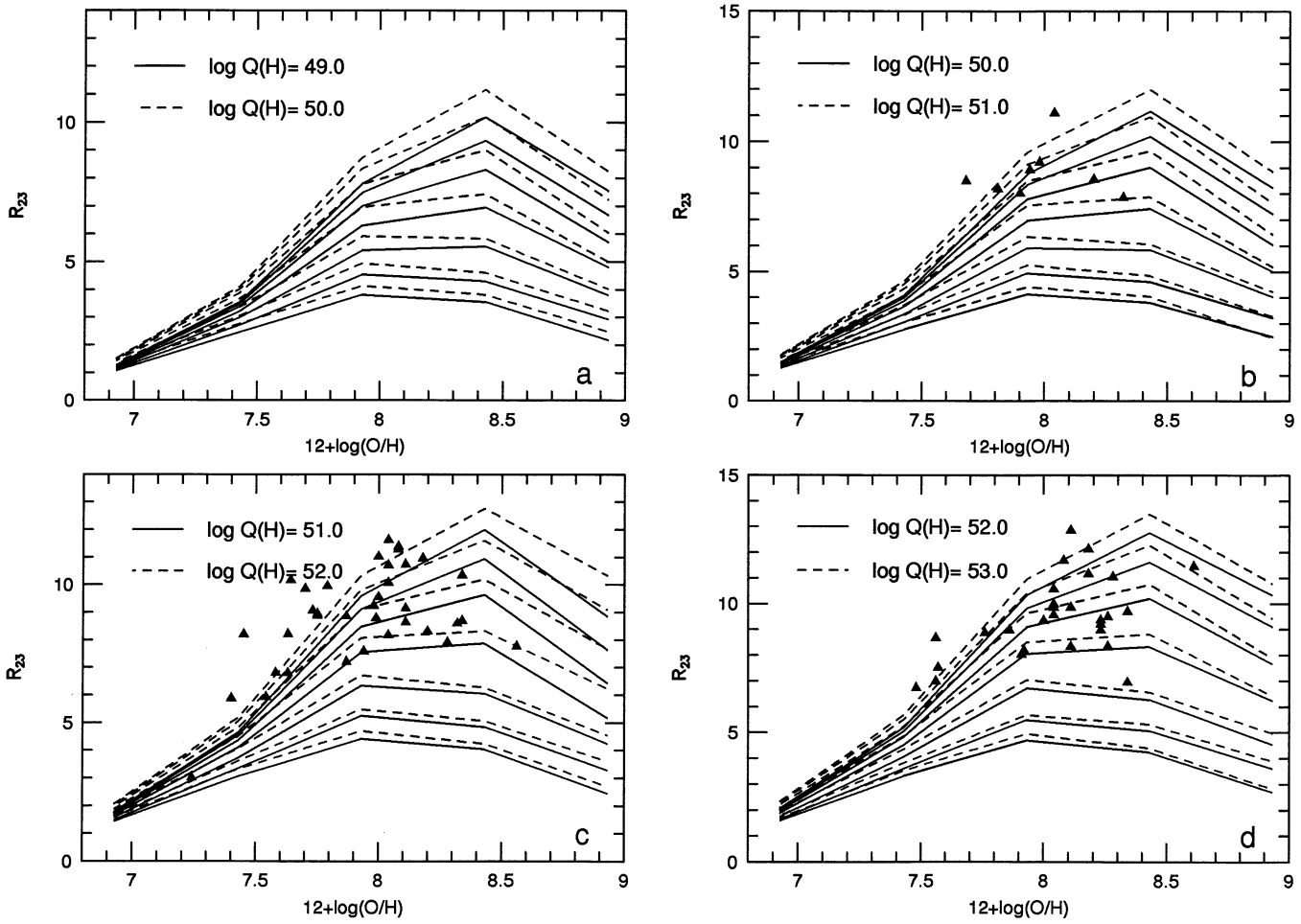

Fig. 10a-d. The R_{23}= ([OII]λ3727 +[OIII]$\lambda\lambda$4959,5007)/Hβ versus oxygen abundance calculated in the interval log $Q(H)$= 49.0-53.0 and divided into four plots. The solid and dashed curves represent different values of log $Q(H)$ for these values of T_{ion}; 55000K (top), 50000K, 47500K, 45000K, 42500K, 40000K, 37500K (bottom). These relations can be used to derive the T_{ion} of H II regions through a method of interpolation provided the abundance of oxygen is known. (the data of the whole range of log $Q(H)$= 45.0-55.0 are available at the CDS via ftp 130.79.128.5). The empirical data are from Masegosa et al. (1994). No objects were found in the range of log $Q(H)$= 49.0-50.0. The position of the blue compact galaxy IZw18 is visualized in Fig. 10c at 12+log(O/H)= 7.24 and data was taken from Davidson and Kinman (1985).

this investigation is the same as the one used by Cerviño and Mas-Hesse (1994). They studied the R_{23} and R_{33} vs. (O/H) relations over four orders of magnitude in log $Q(H)$. They used model stellar atmospheres of Mihalas (1972) of solar chemical composition over a wide range of nebular oxygen abundances, i.e. 6.9 $\leq$12+log(O/H)$\leq$ 8.9. In this analysis these relations were calculated over a range of ten orders of magnitude in log $Q(H)$. Also, model stellar atmospheres of chemical compositions over the whole range of nebular oxygen abundance have been used, i.e. from 1/100 $Z_\odot$ to $Z_\odot$. This is a more realistic approach since the massive stars, which are the nature of the nebular emission, are young and have therefore chemical compositions close to those of the nebular gas out of which they formed. The result of calculations in the interval log $Q(H)$= 49.0-53.0 are shown in Fig. 10a-d and 11a-d for illustration purposes.

The T_{ion} is presented in the range of 37500-55000K for R_{23} and R_{33}, respectively. (the whole range of data in the interval log $Q(H)$= 45.0-55.0 are available via anonymous ftp). These relations can then be used in order to derive the T_{ion} for objects in which the [OIII]λ4363Å line is measurable with known quantities of the $Q(H)$, R_{23}, R_{33} and relative oxygen abundance. It is achieved by first selecting the corresponding range in log $Q(H)$ and from its specific value by interpolating between the curves. This exercise was performed on the sample of Masegosa et al. (1994) as well as on the blue compact galaxy IZw18 (Davidson and Kinman, 1985). This object is the most metal-poor star forming galaxy known to date (12+log(O/H)= 7.24) and has been included in the following in order to widen the range in oxygen abundance. The data of Masegosa et al. was selected because of its homogeneity. The distances were determined assuming a value of the Hubble parameter of H_o= 75 kms^{-1} Mpc^{-1}. The T_{ion}'s derived from R_{33} should, in principle, be less reliable than those derived using R_{23}. This is due to uncertainties in the measurement of the [OIII]λ4363Å line. An acceptable agreement between the two methods was found for $\sim$ 40% of the objects. This means that the deviation in T_{ion} was

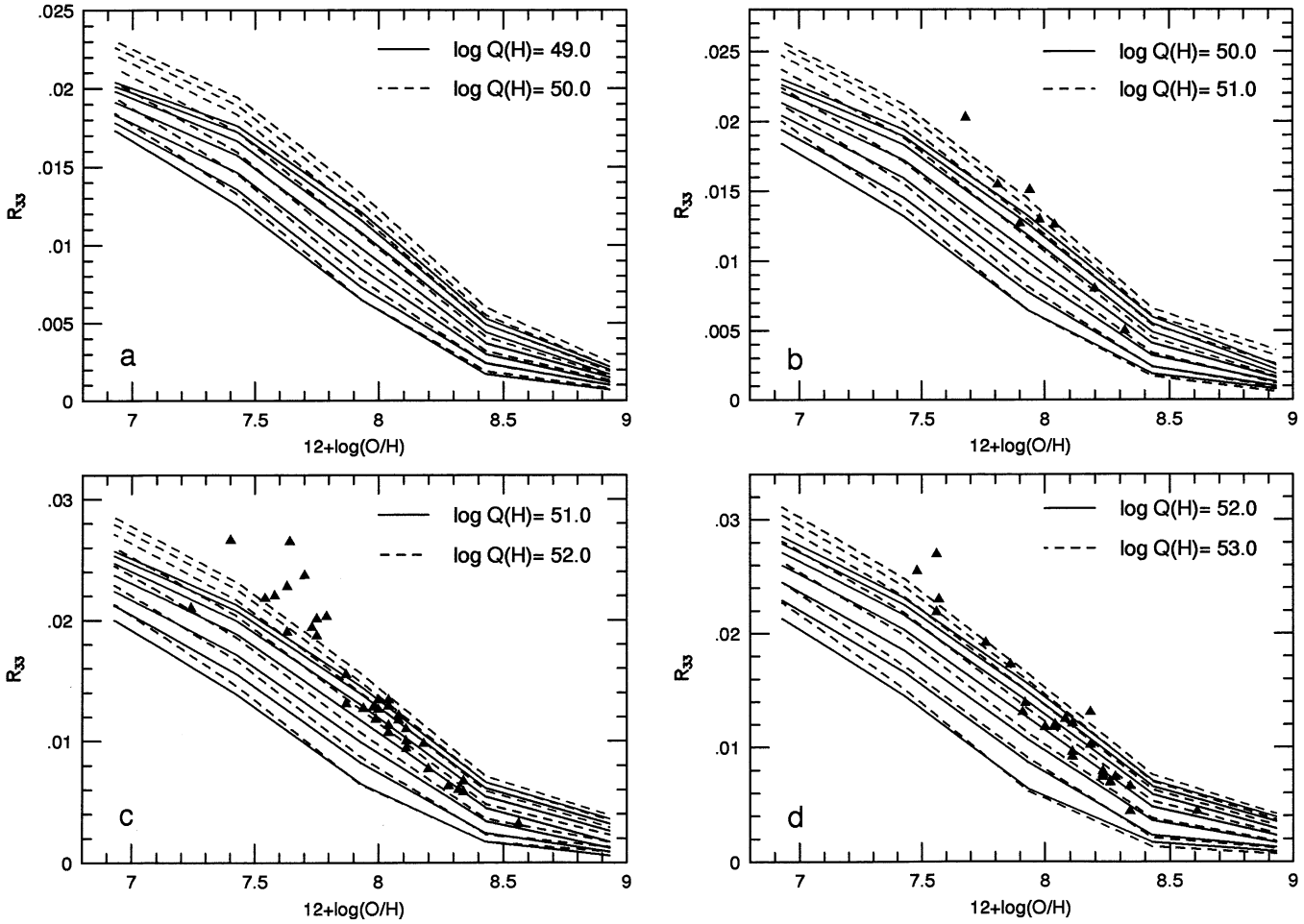

Fig. 11a–d. The R_{33}= [OIII]λ4363/[OIII]$\lambda\lambda$(4959+5007) versus oxygen abundance calculated in the interval log $Q(H)$= 49.0-53.0 and divided into four plots. The solid and dashed curves represent different values of log $Q(H)$ for these values of T_{ion}; 55000K (top), 50000K, 47500K, 45000K, 42500K, 40000K, 37500K (bottom). These curves can be used to derive the T_{ion} of H II regions through a method of interpolation provided the abundance of oxygen is known. (the data of the whole range of log $Q(H)$= 45.0-55.0 are available at the CDS via ftp 130.79.128.5). The empirical data are from Masegosa et al. (1994). No objects were found in the range of log $Q(H)$= 49.0-50.0. The position of the blue compact galaxy IZw18 is visualized in Fig. 11c at 12+log(O/H)= 7.24 and data was taken from Davidson and Kinman (1985).

no more than 2000K. From the theoretical curves in Figs. 10 and 11 one can note that the most decisive temperature estimates result if the R_{23} vs. oxygen abundance relation is used and if 12+log(O/H)$\geq$ 8, roughly. The figures also reveal that the empirical data tend to be located above the theoretical curves at low values of the abundances of oxygen indicating that the $T_{ion} > 55000$K in these objects. This is especially true in the case of R_{33} as evident from Fig. 11. The same trend was noted in the results of Cerviño and Mas-Hesse (1994) and the reason for this is unclear. It could be the result of some systematic errors in the measurement of these lines (see Sect. 3.1) or that the photoionization code fails in predicting the strength of emission lines at low chemical abundances. The possible influence of insufficiencies in the evolutionary tracks and model stellar atmosphere spectra could perhaps be responsible for part of the discrepancies.

3.4.3. The oxygen abundance calibration

The linear R_{23} vs. 12+log(O/H) relation for the empirical sample is given in Fig. 12a-d in various intervals of T_{ion} (the range T_{ion}= 40000-42500K is not presented with a figure since it only contained three objects, the linear-correlation coefficient is r= 0.983 in this case). The temperatures derived are based on R_{23}, only, in order to ensure a large enough sample. This resulted in temperature estimates of about 85% of the objects of Masegosa et al. (1994). For the others ambiguous determinations resulted and they were therefore rejected. The T_{ion} for IZw18 was found to be $\sim$43650K which places this object in the interval of 42500-45000K (Fig. 12a). It is interesting to note that Dufour et al. (1988) compared the strength of a large number of emission lines with respect to Hβ, from the FUV to the optical spectral region, of this object with their photoionization models and concluded that the best agreement was found if 87% of the luminosity in the Hβ line emerged from a component with T_{ion}= 45000K and

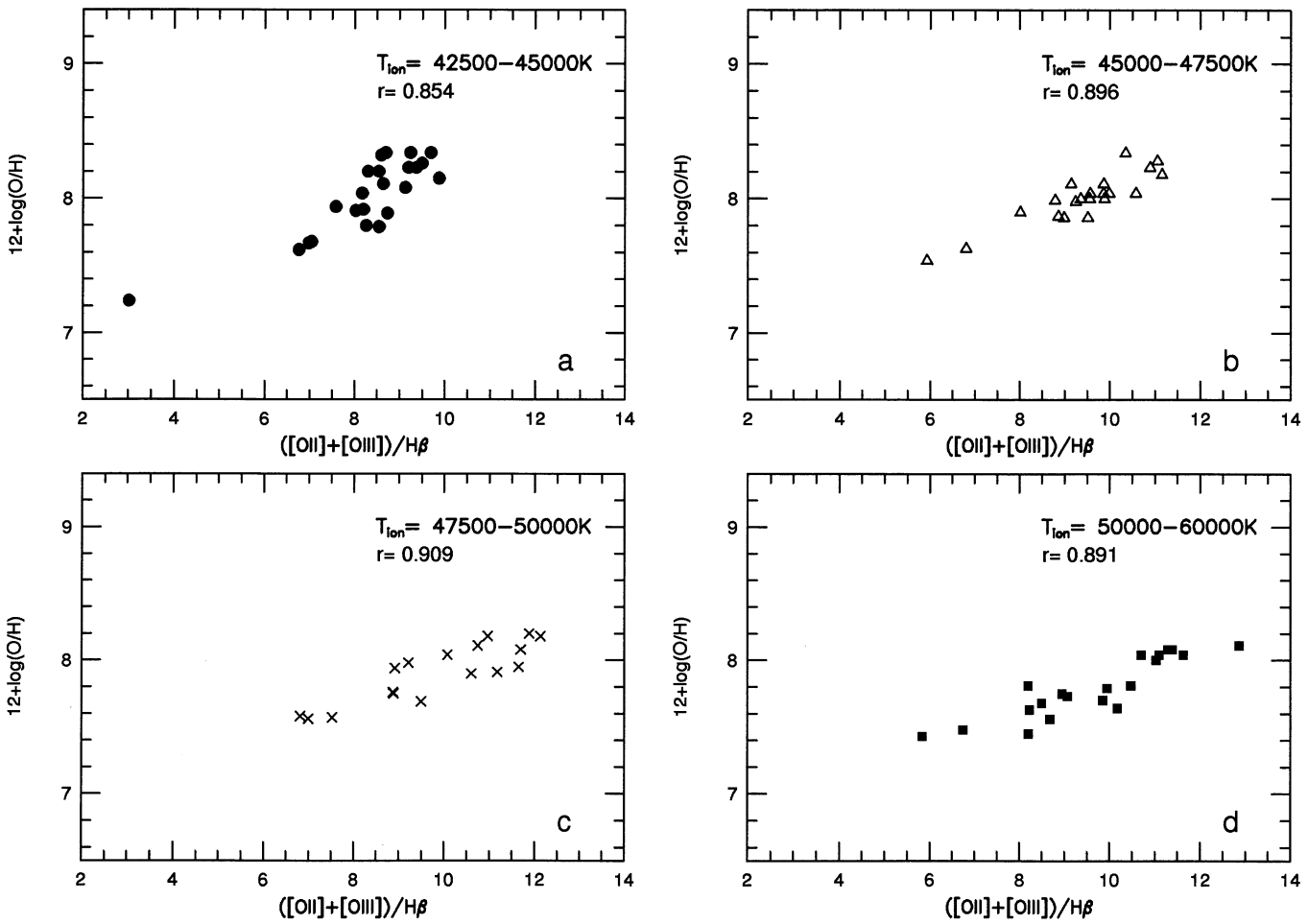

Fig. 12a–d. The objects of Masegosa et al. (1994) as well as Davidson and Kinman (1985) (the object IZw18 shown in Fig. 12a at 12+log(O/H)= 7.24) plotted in intervals of T_{ion} in the R_{23} versus oxygen abundance plane. Linear analytical relations are given in the text. The linear-correlation coefficient is given by r in each case. The range T_{ion}= 40000-42500K is not plotted due to the small number of objects (three) in this range (r= 0.983).

13% from a component with T_{ion}= 35000K which gives a good agreement with the temperature derived in this analysis. At least it indicates that $T_{ion} \leq$ 45000K in the observed H *II* region in this object. For each of these intervals of T_{ion} a linear least-square fit has been applied and the linear-correlation coefficient is given by r in each case. All of these relations comply to the lower branch. The fits are the following

$40000K < T_{ion} < 42500K$

$12 + log(O/H) = 0.19R_{23} + 6.52,\ (r = 0.983)$

$42500K < T_{ion} < 45000K$

$12 + log(O/H) = 0.17R_{23} + 6.62,\ (r = 0.854)$

$45000K < T_{ion} < 47500K$

$12 + log(O/H) = 0.13R_{23} + 6.76,\ (r = 0.895)$

$47500K < T_{ion} < 50000K$

$12 + log(O/H) = 0.11R_{23} + 6.80,\ (r = 0.909)$

$50000K < T_{ion} < 60000K$

$12 + log(O/H) = 0.11R_{23} + 6.69,\ (r = 0.891)$

One should note that, for T_{ion}'s above 47500K, the slope of the linear relations are the same (Fig. 12c and d) indicating that the R_{23} vs. 12+log(O/H) relation is rather insensitive to variations in temperature if the latter is high enough. This is also supported by the theoretical calculations of the lower branch (cp. Fig. 8). The arbitrary choice of 60000K as the upper temperature limit is therefore acceptable even though the existence of objects with higher T_{ion}'s can not be excluded. A calibration of the upper branch has been obtained by shifting the theoretical curves of the lower branch to the empirical data, according to the analytical expressions given, for each temperature range. It is feasible because the shape of the curves remains unaltered. Additional calculations of stellar populations with "top-heavy" IMF's were necessary to invoke in order to account for the objects with the highest temperatures (cp. Fig. 7a).

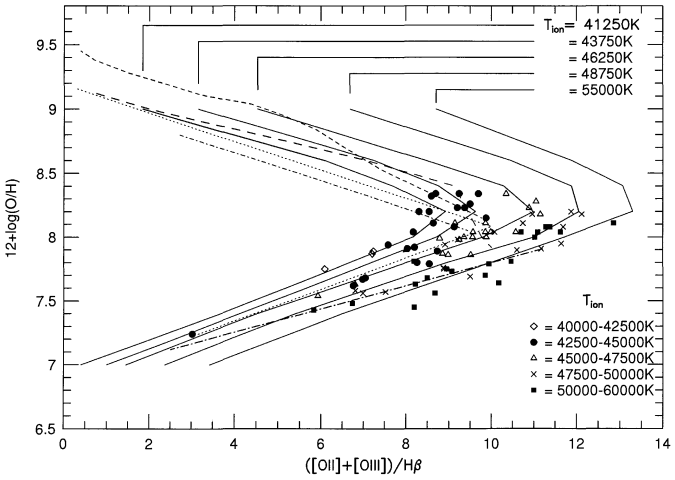

Fig. 13. The calibrated R_{23} versus oxygen abundance relation. The theoretical curves of the lower branch are fitted to the empirical sample separated by different values of the mean temperature of each interval of T_{ion} (solid lines). The resulting analytical expressions for the lower and upper branches, in intervals of T_{ion}, are presented in the text. Some published calibrations are also shown; (···) Edmunds and Pagel (1984), (– –) McCall et al. (1985), (— —) Dopita and Evans (1986), (– · –) Torres-Peimbert et al. (1989), (— · —) Skillman (1989).

The result is visualized in Fig. 13 where the theoretical curves are presented with their mean values of T_{ion} for each interval. It resulted in the following relations for the upper branch

$$40000K < T_{ion} < 42500K$$

$$12 + log(O/H) = -0.10R_{23} + 9.19,\ R_{23} < 6.09$$

$$12 + log(O/H) = -0.12R_{23} + 9.34,\ 6.09 \leq R_{23} < 7.70$$

$$42500K < T_{ion} < 45000K$$

$$12 + log(O/H) = -0.10R_{23} + 9.32,\ R_{23} < 7.25$$

$$12 + log(O/H) = -0.13R_{23} + 9.55,\ 7.25 \leq R_{23} < 8.76$$

$$45000K < T_{ion} < 47500K$$

$$12 + log(O/H) = -0.10R_{23} + 9.45,\ R_{23} < 8.47$$

$$12 + log(O/H) = -0.14R_{23} + 9.79,\ 8.47 \leq R_{23} < 9.85$$

$$47500K < T_{ion} < 50000K$$

$$12 + log(O/H) = -0.10R_{23} + 9.67,\ R_{23} < 10.46$$

$$12 + log(O/H) = -0.14R_{23} + 10.05,\ 10.46 \leq R_{23} < 11.89$$

$$50000K < T_{ion} < 60000K$$

$$12 + log(O/H) = -0.12R_{23} + 10.06,\ R_{23} < 11.89$$

$$12 + log(O/H) = -0.17R_{23} + 10.61,\ 11.89 \leq R_{23} < 13.07$$

For the sake of comparison some other calibrations found in the literature are presented in Fig. 13. These are based on empirical as well as theoretical results and were taken from the following sources; Edmunds and Pagel (1984), McCall et al. (1985), Dopita and Evans (1986), Torres-Peimbert et al. (1989) and Skillman (1989). Another more recent calibration was performed by McGaugh (1991). His results are not shown in the figure but matched the ones presented above rather well. One can note from the figure that, generally, the calibration derived in this investigation coincide rather well with the earlier attempts. Especially the slopes of the curves on the lower and upper branches match very well except the one derived by Skillman (1989) for the lower branch which tends to be more flat than the ones suggested in this investigation. The reason for this is probably that Skillman gave much emphasis to the low metallicity object IZw18 which means that, on the basis of these results, his empirical relation is not based on equivalent T_{ion}'s. One can note that, on the upper branch, the published calibrated curves seem to be located on the lower temperature end of the calibration derived in this analysis i.e. they show indications of T_{ion}'s of about 43000K or lower. This can be understood in the following way. The sample of H *ii* galaxies of Masegosa et al. (1994) includes many objects with unusually high excitation i.e. they show indications of a "top-heavy" IMF or equally a high T_{ion}. They are all low abundance objects and are located on the lower branch and the turn-over region of the R_{23} vs. oxygen abundance relation (see Fig. 1). The empirical and semi-empirical calibrations of Edmunds and Pagel (1984), McCall et al. (1985) and Torres-Peimbert et al. (1989) are based on observations of H *ii* regions in relatively nearby spiral galaxies. One way of interpreting this result would be to claim that these H *ii* regions contain a smaller amount of massive stars, or that the upper mass end is truncated, compared to the sample of Masegosa et al. However, another more reasonable interpretation is at hand. Studying the chemical abundances derived for these objects one sees that they are quite high which therefore places them on the upper branch. As discussed in Sect. 3.2, a massive star of low metallicity remains at higher effective temperature compared to a star of higher metallicity which would therefore account for their relatively low T_{ion}'s. By comparing the calibration derived in this analysis with the theoretical one of Dopita and Evans (1986) one also finds that it is situated on the lower temperature end. The reason is probably that they used input parameters for their model which were chosen in order to nearly match those of the previous (low temperature) empirical or semi-empirical calibrations.

It is difficult to place errorbars on theoretical work. The errors involved are inherent in the theory of stellar evolution, model stellar atmospheres and the model of photoionization used. Judging from the scatter in the value of 12+log(O/H) of the empirical sample alone the errors are estimated to $\sim \pm 0.1$ dex. The true errors are probably larger than this. Finally, no calibration of the turn-over region was performed due to the large scatter in this area as well as to the ambiguous oxygen abundances deduced.

4. Conclusions

A model of spectral evolution of star forming galaxies has been developed. The model is based on stellar evolutionary tracks and model stellar atmosphere spectra of various metallicities. Stellar populations and nebular components of eleven different metallicities were used in the calculations. These were contained in the interval; $7.0 \leq 12+\log(O/H) \leq 9.0$. The aim has been to study the relation between the optical emission line ratio R_{23}= ([OII]+[OIII])/Hβ and the nebular oxygen abundance for which empirical results show some interesting trends. The active and post-active phases of a single burst of star formation of various nebular chemical compositions were analyzed. It was shown that the scatter in the empirical comparison sample in the so called turn-over region could be an effect of temporal evolution of the underlying stellar population, only, although various filling factors in the nebular gas could explain part of it. Various upper stellar mass limits or slopes of the IMF in the objects producing the nebular component would give the same effect. It was found that the evolution of R_{23}, once the star formation has ceased, is very rapid. Depending on the IMF used and the metallicity of the gas from which the stars was formed it was shown that the nebular emission diminishes no later than about 20-30 Myr after the termination of star formation. This is due to the short lifetimes of the most massive stars. The R_{23} vs. oxygen abundance relation offers a possibility to deduce the oxygen abundance in a star forming region in the lack of the temperature-sensitive emission line [OIII]λ4363Å. Therefore, a calibration of the upper branch, based on a fit of theoretical curves to empirical data of the lower branch, was attempted.

Acknowledgements. This work was supported by the Swedish Natural Science Research Council. Dr. Ferland is thanked for the availability of his photoionization code CLOUDY. Drs. Nils Bergvall and Jari Rönnback are thanked for giving constructive criticism on a draft version of this paper. The referee, Dr. Mas-Hesse, is thanked for many comments and suggestions which have improved the quality of this article.

References

Alloin, D., Collin-Souffrin, S., Joly, M., Vigroux, L., 1979, A&A 78, 200
Bica, E., Alloin, D., Schmidt, A., 1990, MNRAS 242, 241
Campbell, A., 1988, ApJ 335, 644
Carlberg, R.G., Couchman, H.M.P, 1989, ApJ 340, 47
Cerviño, M., Mas-Hesse, J.M., 1994, A&A 284, 749
Charbonnel, C., Meynet, G., Meader, A., Schaller, G., Schaerer, D., 1993, A&AS 101, 415
Charlot, S., Bruzual, G.A., 1991, ApJ 367, 126
Ciardullo, R.B., Demarque, P., 1977, Trans. Astr. Obs. Yale University Vol. 35
Clegg, R.E.S, Middlemass, D., 1987, MNRAS 228, 759
Davidson, K., Kinman, T.D., 1985, ApJS 58, 321
De Young, D.S., Gallagher, J.S. III, 1990, ApJ 356, L15
De Young, D.S., Heckman, T.M., 1994, ApJ 431, 598
Díaz, A.I., 1988, MNRAS 231, 57
Dinerstein, H.L., 1989, 'The Interstellar Medium in Galaxies', eds. Thronson, Jr., H.A., Shull, J.M., Kluwer Academic Publishers p.257
Dopita, M.A., Evans, I.N., 1986, ApJ 307, 431
Dufour, R.J., Garnett, D.R., Shields, G.A., 1988, ApJ 332, 752
Edmunds, M.G., Pagel, B.E.J., 1984, MNRAS 211, 507
Evans, I.N., Dopita, M.A., 1985, ApJS 58, 125
Evans, I.N., 1986, ApJ 309, 544
Evans, I.N., 1991, ApJS 76, 985
Ferland, G.J., Truran, J.W., 1981, ApJ 244, 1022
Ferland, G.J., 1993, University of Kentucky Departments of Physics and Astronomy, Internal Report
García-Vargas, M.L., Bressan, A., Díaz, A.I., 1995, preprint
Garnett, D.R., Shields, G.A., 1987, ApJ 317, 82
Gerola, H., Seiden, P.E., Schulman, L.S., 1980, ApJ 242, 517
Grossman, A.S., Graboske, Jr, H.C., 1971, ApJ, 164, 475
Howarth, I.D., Lynas-Gray, A.E., 1989, MNRAS 240, 513
Hummer, D.G., Mihalas, D., 1970, MNRAS 147, 339
Kinman, T.D., Davidson, K., 1981, ApJ 243, 127
Kudritzki, R.P., Gabler, R., Kunze, D., Pauldrach, A. W.A., Puls, J. 1991, 'Massive Stars in Starbursts', eds. Leitherer, C., Walborn, N.R., Heckman, T.M., Norman, C.A., Cambridge University Press, p. 59
Kunth, D., Sargent, W.L.W, 1983, ApJ 273, 81
Kunth, D., Maurogordato, S., Vigroux, L., 1988, A&A 204, 10
Kurucz, R.L., 1979, ApJS 40, 1
Kurucz, R.L., 1992, 'The Stellar populations in Galaxies', eds.: Barbuy, B., Renzini, A., Kluwer Academic Publishers, p. 225
Kwitter, K.B., Aller, L.H., 1981, MNRAS 195, 939
Maeder A., 1991, Publications de L'Observatoire de Genéve No. 84
Maeder A., 1995, private communication
Martin, P., Roy, J.-R., 1992, ApJ 397, 463
Masegosa, J., Moles, M., Campos-Aguilar, A., 1994, ApJ 420, 576
McCall, L.M., 1982, Ph.D. thesis, University of Texas
McCall, L.M., Rybski, P.M., Shields, G.A., 1985, ApJS 57, 1
McGaugh, S.S., 1991, ApJ 380, 140
Melnick, J., Terlevich, R.J., Eggleton, P.P, 1985, MNRAS 216, 255
Mihalas, D., 1972, NCAR Technical Note NCAR-TN/STR 76, National Center for Atmospheric Research, Boulder
Olofsson, K., 1989, A&AS 80, 317
Olofsson, K., 1995a, A&AS 111, 57
Olofsson, K., 1995b, A&A 293, 652
Olofsson, K., 1996, 'From Stars to Galaxies: The Impact of Stellar Physics on Galaxy Evolution', eds. C. Leitherer, U. Fritze-von Alvensleben, J. Huchra, ASP Conf. Series Vol. 98, p. 77
Osterbrock, D.E., 1989, 'Astrophysics of Gaseous Nebulae and Active Galactic Nuclei', University Science Books
Pagel, B.E.J., Edmunds, M.G., Blackwell, D.E., Chun, M.S., Smith, G., 1979, MNRAS 189, 95
Pagel, B.E.J., Edmunds, M.G., Smith, G., 1980, MNRAS 193, 219
Peimbert, M., Peña, M., Torres-Peimbert, S., 1986, A&A 158, 266
Pilyugin, L.S., 1992, A&A 260, 58
Salpeter, E.E., 1955, ApJ 121, 161
Salzer, J.J., Alighieri, S.D.S, Matteucci, F., Giovanelli, R., Haynes, M.P., 1991, AJ 101, 1258
Scalo, J.M., 1986, 'Fundamentals of Cosmic Physics', no. 11
Scalo, J.M., 1987, 'Starbursts and Galaxy Evolution', eds. T.H. Thuan, T. Montmerle, J. Tran Thahn Van, Les Arcs, p.445
Scalo, J.M., 1990, 'Windows on Galaxies', eds. G. Fabbiano, J.S. Gallagher III, A. Renzini, Kluwer Academic Publishers, p.125
Schaerer, D., Meynet, G., Maeder, A., Schaller,, G., 1993a, A&AS 98, 523

Schaerer, D., Charbonnel, C., Meynet, G., Maeder, A., Schaller, G., 1993b, A&AS 102, 339
Schaller,, G., Schaerer, D., Meynet, G., Maeder, A., 1992, A&AS 96, 269
Shields, G., Searle, L., 1978, ApJ 222, 821
Skillman, E.D., Melnick, J., Terlevich, R., Moles, M., 1988, A&A 196, 31
Skillman, E.D., 1989, ApJ 347, 883
Skillman, E.D., Kennicutt, R.C., Hodge, P.W., 1989a, ApJ 347, 875
Skillman, E.D., Terlevich, R., Melnick, J., 1989b, MNRAS 240, 563
Stasińska, G., 1980, A&A 84, 320
Stasińska, G., 1982, A&AS 48, 299
Stauffer, J.R., Bothun, G.D., 1984, AJ 89, 1702
Talent, D.L., 1983, PASP 95, 986
Terlevich, R., Melnick, J., Masegosa, J., Moles, M., Copetti, M.V.F., 1991, A&AS 91, 285
Thielemann, F.-K., Nomoto, K., Hashimoto, M., 1993, 'Origin and Distribution of the Elements' eds. N. Prantzos, E. Vangioni-Flam, M. Casse, Cambridge University Press, p. 297
Torres-Peimbert, S., Peimbert, M., Fierro, J., 1989, ApJ 345, 186
VandenBerg, D.A., 1985a, ApJS 58, 561
VandenBerg, D.A., 1985b, ApJS 58, 711
VandenBerg, D.A., 1986, private communication
Vílchez, J.M., Pagel, B.E.J., 1988, MNRAS 231, 257
Vílchez, J.M., Pagel, B.E.J., Díaz, A.I., Terlevich, E., Edmunds, M.G., 1988, MNRAS 235, 633
Walsh, J.R., Roy,J.-R., 1989, ApJ 341, 722
Webster, B.L., Smith, M.G., 1983, MNRAS 204, 743
White S. D. M. 1989, 'The Epoch of Galaxy Formation', eds. C.S. Frenk, R.S. Ellis, T. Shanks, A.F. Heavens and J.A. Peacock, Kluwer Academic Publishers, p. 15
Whitworth A., 1979, MNRAS 186, 59
Woosley, S.E., Weaver, T.A., 1995, ApJS 101, 181
Zaritsky, D., Elston, R., Hill, J.M., 1990, AJ 99, 1108

This article was processed by the author using Springer-Verlag LaTeX A&A style file *L-AA* version 3.